Eikonal approximation in heavy-ion fragmentation reactions

H. Esbensen
Physics Division, Argonne National Laboratory, Argonne, Illinois 60439

G. F. Bertsch
Institute for Nuclear Theory, University of Washington, Seattle, Washington 98195
(Received 23 March 2001; published 13 June 2001)

Projectile fragmentation reactions are well suited to structure studies of weakly bound nuclei, but an accurate reaction theory is necessary to extract quantitative spectroscopic properties. We examine here the accuracy of the commonly used eikonal approximation for the nuclear-induced breakup of halo nuclei. Comparing to numerical solutions of the full time-dependent Schrödinger equation, we find that the eikonal remains fairly accurate for calculating breakup probabilities of halo nuclei even down to 20 MeV/nucleon, reproducing relative spectroscopic strengths to within a few percent. Absolute reaction probabilities tend to be underpredicted by the eikonal, which would make extracted spectroscopic strengths somewhat too high. We discuss other features that are seen in the full calculation but are missing in the eikonal approximation such as the ''towing'' mode.

DOI: 10.1103/PhysRevC.64.014608 PACS number(s): 24.10.−i, 25.60.−t

I. INTRODUCTION

A wide variety of reaction models have been developed and applied to analyze breakup reactions of halo nuclei. A popular model is the eikonal approximation [1–5], which is very convenient from a computational point of view but is only justified at higher beam energies. Since many fragmentation experiments have been performed in the energy range of 20–60 MeV/nucleon and the data are often analyzed using the eikonal approximation (see for example Refs. [6–10]) it is of interest to assess its accuracy and determine the range of beam energies for which it is reliable.

In this work we test the eikonal approximation by comparing it to numerical solutions of the full time-dependent Schrödinger equation for a halo neutron in a projectile interacting with a nuclear target as well as the core of the projectile. For given interactions, the only approximation is a classical treatment of the projectile-target coordinate, which is quite safe for the heavy-ion reactions considered. We previously used the time-dependent Schrödinger method to study higher-order effects in Coulomb dissociation [11–13]. For our tests here, we calculate the nuclear-induced breakup of the halo nucleus ^{11}Be. The time-dependent Schrödinger equation has also been applied to halo breakup by other authors [14–16]. They use numerical techniques that are different from the one we have used to solve the equation. In any case, it is now computationally feasible to solve the time-dependent Schrödinger equation by several methods to sufficient accuracy that the numerical aspect is not a real limitation on the applicability.

Besides the eikonal and time-dependent Schrödinger equation, a number of other approaches have been used to describe heavy-ion breakup reactions. The transfer-to-continuum model [17] is as convenient as the eikonal and is in some ways more accurate. However, it is not applicable with standard-range optical potentials such as those used here, and so we do not attempt to include it in our comparison. Another approach that avoids the approximations of the eikonal is the continuum discretized coupled channels method [18–20]. In principle, the equations solved by this method are exact, but the computational demands are severe. Many continuum states must be included in the basis. Also, coupling between the continuum states cannot be neglected, as is sometimes done, and still have reliable results [21].

II. HAMILTONIAN AND DYNAMIC EQUATIONS

We consider a model in which the only coordinates are the neutron's and the projectile-target coordinate **R**. The latter is treated classically, and for simplicity we assume a straight-line trajectory $\mathbf{R}(t)=\mathbf{b}+\mathbf{v}t$. This leaves the neutron-core and neutron-target potentials to be specified, whereas the core-target interaction is set to zero. Again for simplicity we ignore spin-orbit interactions, taking the neutron-core potential U_{nc} to have a simple Woods-Saxon form,

$$U_{nc}(r)=-V_c f\left(\frac{r-R_c}{a_c}\right), \tag{1}$$

where $f(x)=(1+e^x)^{-1}$. The initial state of the neutron $|0\rangle$ is an eigenstate of the potential; for ^{11}Be we choose the parameters so that the eigenenergy of the second s-wave bound state equals the empirical separation energy of 0.5 MeV. We use $V_c=61.1$ MeV, $R_c\approx 2.7$ fm, and $a_c=0.52$ fm the precise value of R_c depends on the coordinate space mesh used to solve the Schrödinger equation.

The neutron-target interaction is parametrized as a conventional optical potential

$$U_{nt}(r_{nt})=-V_0 f\left(\frac{r_{nt}-R_0}{a_0}\right)-i\left[W_{v0} f\left(\frac{r_{nt}-R_w}{a_w}\right)-4W_{s0} f'\left(\frac{r_{nt}-R_w}{a_w}\right)\right], \tag{2}$$

where $f'(x)=df(x)/dx$. Here we have employed the energy-dependent parameters determined in Ref. [23]. The interaction (2) acts on the coordinates **r** for the relative motion of the neutron and the ^{10}Be core through the neutron-target distance $r_{nt}=|\mathbf{R}(t)-\alpha\mathbf{r}|$, where $\alpha=A_c/(A_c+1)$ and $A_c=10$ is the core mass.

The immediate object of the reaction calculation is the neutron wave function in the final state. In the eikonal approximation, which assumes that the target interaction has a very short duration, the final state wave is obtained by a simple multiplicative factor. In the present model, this is

$$\Psi_f(\mathbf{r})=S_{nt}(|\mathbf{b}-\alpha\mathbf{r}_\perp|)|0\rangle = \exp\left(\int_{-\infty}^{\infty}\frac{dz}{i\hbar v}U_{nt}(\sqrt{|\mathbf{b}-\alpha\mathbf{r}_\perp|^2+z^2})\right)|0\rangle, \quad (3)$$

where $|0\rangle$ is the initial ground state wave function, and v is the projectile velocity.

For the full dynamics we integrate the time-dependent Schrödinger equation over a time interval $-T<t<T$ where $t=0$ at closest approach and T is chosen large enough to cover the duration of the interaction with the target. Numerically, we represent the neutron-core wave function in a spherical basis centered on the core of the projectile,

$$\Psi(\mathbf{r},t)=\frac{1}{r}\sum_{lm}u_{lm}(r,t)Y_{lm}(\hat{r}). \quad (4)$$

This gives the following set of coupled equations,

$$i\hbar\frac{d}{dt}u_{lm}(r,t)=\left[\frac{\hbar^2}{2m_0}\left(-\frac{d^2}{dr^2}+\frac{l(l+1)}{r^2}\right)+U_{nc}(r)\right]u_{lm}(r,t)+C_{lm}(r,t), \quad (5)$$

where m_0 is the neutron-core reduced mass. The last term is the coupling generated by the neutron-target interaction,

$$C_{lm}(r,t)=\sum_{l'm'}\langle Y_{lm}|U_{nt}[|\mathbf{R}(t)-\alpha\mathbf{r}|]|Y_{l'm'}\rangle u_{l'm'}(r,t). \quad (6)$$

The coupling is calculated by a multipole expansion of the interaction U_{nt}.

It is convenient to take the z axis (or m-quantization axis) perpendicular to the scattering plane, the x axis in the direction of the impact parameter **b**, and the y axis in the direction of **v**. We exploit the reflection symmetry with respect to the scattering plane, which permits us to restrict the sum in Eq. (4) to terms with even or odd values of $l+m$ depending on whether $l+m$ is even or odd in the initial state.

We now discuss purely numerical aspects of solving the equations. We use the finite difference method to integrate Eq. (5), which was described in connection with Eq. (6) of Ref. [11]. An important parameter in this method is

$$\tau=\frac{\hbar\Delta t}{4m_0(\Delta r)^2}, \quad (7)$$

where Δr is the radial step, and Δt is the time step. This parameter should be of the order of one in order to achieve a reasonably converged result. We have chosen the radial step $\Delta r=0.2$ fm, and a maximum r between 50 and 100 fm. To calculate breakup probabilities, it is sufficient to use $r_{max}=50$ fm but to get realistic momentum distributions one needs a larger r_{max}. The integration is started with the projectile-target y separation specified at some value $y_0=-vT$, and the time integration is performed up to a time $+T$. Since there is no Coulomb interaction, one does not have to cover a large range of spatial separations; in the present case the range $-40<y<40$ fm gives ample accuracy.

Concerning the decomposition into l and m, we find that it is adequate to limit the channels to $l\leqslant l_{max}=12$ as will be seen below. For the s-wave halo orbital, the number of (lm) channels is 91 taking the scattering plane symmetry into account. This is about the most we are able to handle within a reasonable computation time. For consistency, we include all contributing terms in the multipole expansion of U_{nt} in Eq. (6), i.e., $\lambda\leqslant 2l_{max}$.

III. OBSERVABLES

Once the final state halo wave function $\Psi_f(\mathbf{r})=\Psi(\mathbf{r},T)$ has been calculated, one can obtain the total one-neutron removal probability as

$$P_{-1n}=1-|\langle 0|\Psi_f\rangle|^2. \quad (8)$$

The one-neutron stripping probability is calculated from the norm of the wave function after the collision according to

$$P_{\rm str}(b)=1-\langle\Psi_f|\Psi_f\rangle. \quad (9)$$

The diffraction dissociation probability is determined as the norm of the continuum part of the wave function after the collision. If the ground state is the only bound state, then the continuum part of the wave function is

$$\Psi_f^{\rm cont}=\Psi_f-|0\rangle\langle 0|\Psi_f\rangle. \quad (10)$$

The diffraction norm is

$$P_{\rm diff}(b)=\langle\Psi_f|\Psi_f\rangle-|\langle 0|\Psi_f\rangle|^2. \quad (11)$$

The two probabilities, Eqs. (9) and (11), add up to Eq. (8).

Besides the integrated diffraction probability, differential probability distributions in the final state are measured and provide important information. To compute momentum distributions, we project the final state wave function onto scattering states of the neutron-core Hamiltonian. We define amplitudes S_{klm} so that the wave function in momentum space is

$$\Psi_f(\mathbf{k})=\frac{1}{k}\sum_{lm}Y_{lm}(\hat{k})S_{klm}(b). \quad (12)$$

Thus the complete final state momentum distribution will be given by

$$\frac{dP(b,\mathbf{k})}{d\mathbf{k}} = |\Psi_f(\mathbf{k})|^2 = \frac{1}{k^2}\left|\sum_{lm} Y_{lm}(\hat{k}) S_{klm}(b)\right|^2. \quad (13)$$

The amplitudes S_{klm} are calculated as overlaps of the final state wave function with the scattering states $|klm\rangle = (1/r)\phi_{kl}(r)Y_{lm}(\hat{r})$. We normalize the radial wave function to

$$\phi_{kl}(r) \to \sqrt{\frac{2}{\pi}} \sin[kr + \delta_l(k) - l\pi/2], \quad \text{for} \quad r \to \infty,$$

where $\delta_l(k)$ is the nuclear phase shift. With this normalization, the amplitudes in Eqs. (12) and (13) are given by

$$S_{klm}(b) = e^{i[\delta_l(k) - l\pi/2]} \int dr \phi_{kl}(r) u_{lm}(r,T). \quad (14)$$

The expressions (9) and (11) are also applied to the eikonal final state wave function Eq. (3). To calculate the momentum distribution (13), we need to make an angular momentum decomposition of the eikonal factor. Here it is convenient to expand $S(\mathbf{b},\mathbf{r}_\perp) - 1$ rather than $S(\mathbf{b},\mathbf{r}_\perp)$ itself, because the integral can then be limited to a cylinder along the target trajectory. The subtraction by one is, in principle, harmless because the continuum states are orthogonal to the ground state. The same procedure can be applied in the time-dependent description, i.e., we use the continuum part of the wave function, Eq. (10), instead of the full solution, when calculating the radial matrix elements Eq. (14).

In our comparative study here we will only consider two components of the momentum distribution, namely, the angle-averaged distribution and the longitudinal momentum distribution. The angle-integrated distribution is closely related to the decay-energy spectrum and it is given by

$$\frac{dP(b,k)}{dk} = \sum_{lm} |S_{klm}(b)|^2. \quad (15)$$

The longitudinal momentum distribution is the projection on the beam direction. This is most conveniently evaluated in a coordinate system with the z axis along the beam direction. The full distribution is again given by Eq. (13) but the amplitudes are replaced by $\tilde{S}_{klm} = \Sigma_{m'} S_{klm'} D^l_{m'm}(\omega)$, where ω is the rotation that brings the old coordinate system (with the y axis in the beam direction) into the new coordinate system (with the z axis in the beam direction). The integration over transverse momenta is much simpler in the new coordinate system because the integration over the transverse ϕ angle gives an expression that is diagonal in m. The resulting distribution is

$$\frac{dP(k_z)}{dk_z} = 2\pi \int_{|k_z|}^{\infty} \frac{dk}{k} \sum_m \left| \sum_{l \geq |m|} Y_{lm}(\theta_k) \tilde{S}_{klm} \right|^2, \quad (16)$$

where θ_k is given by $\cos\theta_k = k_z/k$.

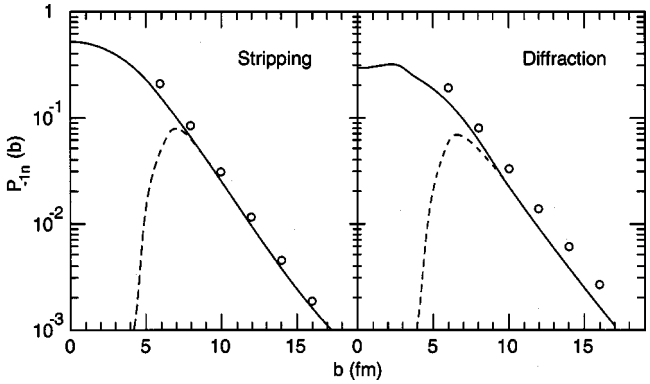

FIG. 1. Stripping and diffraction dissociation probabilities as functions of the impact parameter b for $^{10}\mathrm{Be} \to {}^{10}\mathrm{Be} + n$ fragmentation on a ^{12}C target at 20 MeV/nucleon. The solid curves show the probabilities from the eikonal model. The circles show the probabilities calculated with the time-dependent Schrödinger equation. The dashed curves show the eikonal result obtained with an additional absorption from an empirical core-target interaction.

IV. RESULTS

In this section we apply the above theory to the $^{11}\mathrm{Be} \to {}^{10}\mathrm{Be} + n$ breakup reaction. We will consider a variety of reaction conditions, particularly examining the beam energy dependence and the dependence on properties of the initial bound state wave function. We first investigated the numerical accuracy of the dynamic calculations, varying the numerical parameters Δr, the time step, and l_{max}. Taking values given in Sec. II, we estimate that the accuracy of the diffraction dissociation probability is of the order of 2% at 20 MeV/nucleon and an impact parameter $b = 8$ fm. We have also calculated the breakup of ^{11}Be at 400 MeV/nucleon. Here we have used a purely imaginary optical potential, which was determined from nucleon-nucleon cross sections and the target density as described in Ref. [4]. At this high energy we would expect a perfect agreement between the eikonal and dynamic calculations. We find that the results agree within 1% which gives us additional confidence in the numerical accuracy of our calculations.

A. Breakup probabilities

We now examine the probabilities for stripping and diffraction dissociation for ^{11}Be, starting with a ^{12}C target and a beam energy of 20 MeV/nucleon. The calculated breakup probabilities are shown in Fig. 1 as functions of the impact parameter. The solid curve is the result from the eikonal approximation, Eq. (3). The dashed curve is the eikonal result, which includes an additional absorption from a core-target interaction (obtained with a folding model). The resulting core profile function causes a strong reduction in the one-neutron removal probability at smaller impact parameters. It is seen that the impact parameter range of about 5–15 fm is responsible for practically the entire cross section. It should also be noted that the absolute cross sections will have a significant uncertainty associated with the core-target profile function.

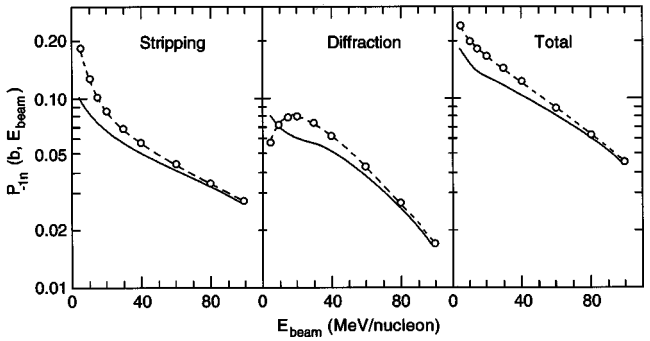

FIG. 2. Breakup probabilities as a function of beam energy for the ^{11}Be reaction on a ^{12}C target at a $b=8$ fm impact parameter. Solid curves show the eikonal result, and circles connected with dashed lines are the results of the full dynamic calculation.

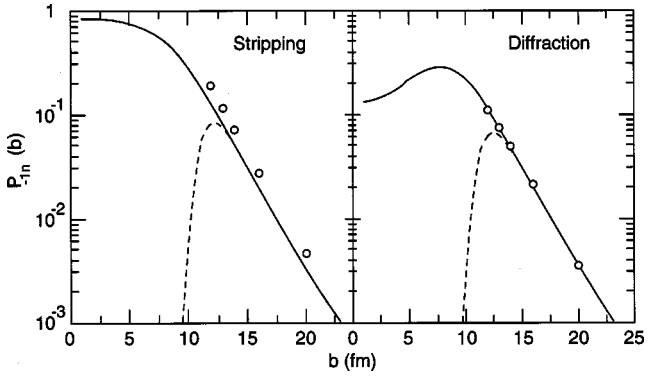

FIG. 4. Breakup probabilities for ^{11}Be as in Fig. 1, but for a ^{208}Pb target at 20 MeV/nucleon.

The dynamic calculation using the time-dependent Schrödinger equation is shown with open circles in Fig. 1. Since the core-target interaction is set to zero in the dynamic calculation, the results should be compared to the solid curves. For both the stripping and diffraction, the eikonal underestimates the probabilities by about 25%, but reproduces the dependence on b quite well. The underprediction of the stripping is easy to understand qualitatively. In the eikonal approximation, the absorptive potential of the target acts only on the halo density in the immediate path. In the full dynamics, there is also a flux from the halo wave function into the target region in response to earlier absorption and diffraction.

The three probabilities (stripping, diffraction, and total) are shown as functions of the beam energy in Fig. 2 for a typical impact parameter $b=8$ fm. One sees the expected trend that the eikonal becomes increasingly accurate as the beam energy increases. The same results are plotted as the ratio of the eikonal to dynamic probabilities in Fig. 3. From perturbation theory, one would expect the eikonal to converge to the full dynamics as $1/v \sim E_{beam}^{-1/2}$ for real potentials and $1/v^2 \sim 1/E_{beam}$ for absorptive potentials. We note that the energy dependence of the optical potential we have used [23] will also affect this behavior. The calculated stripping probabilities follow the expected dependence above $E_{beam}=20$ MeV/nucleon; the ratio of probabilities is quite well fit by the function $P_{eik}/P_{dyn}=1-E_x/E_{beam}$ with $E_x=4.5$ MeV. The diffraction probability has a similar trend but it fluctuates erratically below 20 MeV/nucleon.

In Figs. 4 and 5 we show the corresponding quantities for the breakup reaction on a heavy target ^{208}Pb. The results are similar; there is a consistent underprediction of the stripping probability in the eikonal approximation, which becomes larger at a lower beam energy. Interestingly, the error in the diffraction does not vary smoothly as a function of beam energy; by accident the eikonal result at 20 MeV/nucleon is quite good. From these results we consider 20 MeV/nucleon

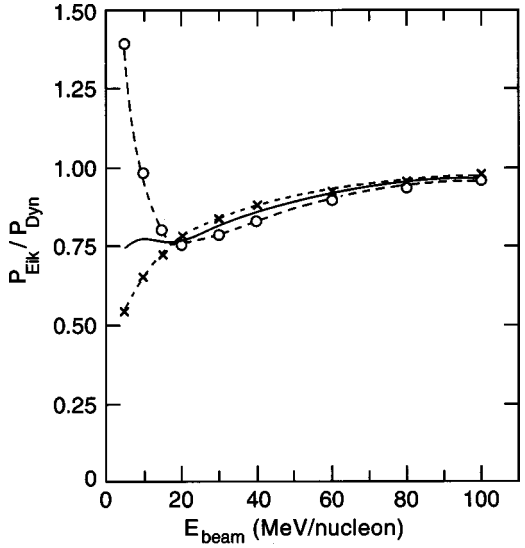

FIG. 3. Comparison of eikonal and dynamic results, presenting the results of Fig. 2 as a ratio of eikonal to dynamic probabilities. The solid curve is the result for the total one-neutron removal probability. The dashed curves are the results for stripping (crosses) and diffraction dissociation (circles).

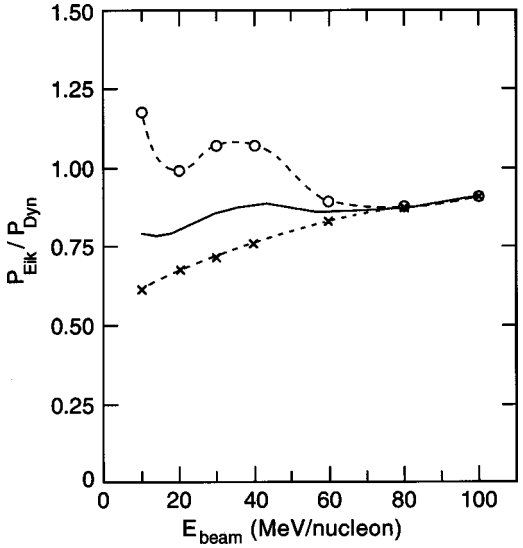

FIG. 5. Ratio of eikonal to dynamic probabilities for a ^{11}Be breakup on a ^{208}Pb target as functions of beam energy, at the impact parameter $b=13$ fm. The solid curve is the result for the total one-neutron removal probability. The dashed curves are the results for stripping (crosses) and diffraction dissociation (circles).

TABLE I. Ratio of eikonal to dynamically calculated one-neutron removal probabilities in ^{11}Be. The table shows different bound state angular momenta l, separation energies S_n, and beam energies E_{beam} for breakup on a ^{12}C target at an impact parameter $b=8$ fm.

E_{beam}	l	$S_n=0.5$ MeV	$S_n=3.0$ MeV
20 MeV/nucleon	0	0.77	0.75
	1	0.77	0.78
	2	0.79	0.82
40 MeV/nucleon	0	0.86	0.84
	1	0.86	0.85
	2	0.86	0.88

a lower boundary for the reliable use of the eikonal approximation.

As mentioned above, the determination of absolute spectroscopic strengths from nuclear breakup is hardly feasible due to the uncertainty in the core-target interaction. A less ambitious use of reaction theory is to apply it only to relative spectroscopic strengths when several final states are possible. To assess the validity of the eikonal for such purposes, we present in Table I the ratio of eikonal and dynamic one-neutron removal probabilities as a function of bound state angular momenta and binding energies. We see that the eikonal is an excellent approximation when used this way. For example, at a beam energy of 40 MeV/nucleon, the difference in the probability ratios is only a few percent over the range of bound state angular momenta from 0 to 2 and binding energies of 0.5 to 3.0 MeV.

B. Angular momentum distributions

The angular momentum distribution of the final state is illustrated in Fig. 6 for a ^{12}C target at three beam energies, again at the impact parameter $b=8$ fm. The solid curves are the eikonal predictions, and the dashed curves are the results of dynamic calculations with $l_{max}=12$. We find that the dynamic calculations have converged quite well at smaller final

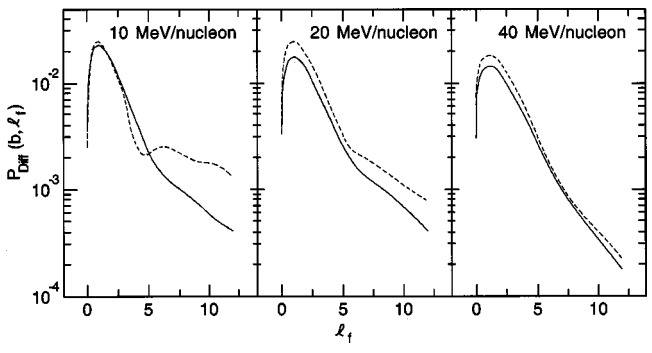

FIG. 6. Angular momentum decomposition of diffraction dissociation probability in the final state. Reaction conditions are the same as in Fig. 2. Results are shown at three beam energies, both in the eikonal approximation (solid curves) and from the dynamic calculation (dashed curves).

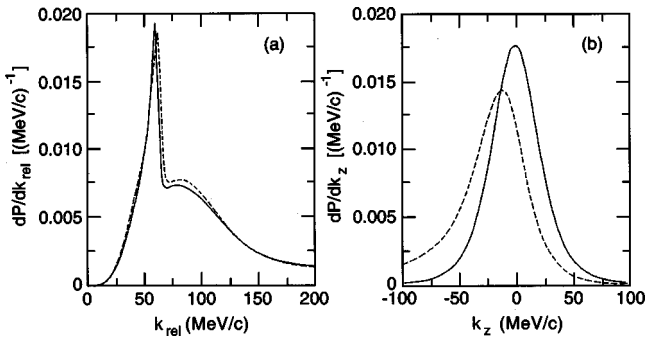

FIG. 7. Momentum distributions of neutrons in the ^{11}Be projectile frame, produced in diffraction dissociation on a ^{12}C target at 20 MeV/nucleon and an impact parameter $b=8$ fm. The angle-integrated distribution is shown in (a), and (b) shows the momentum distribution projected onto the beam direction. The solid and dashed curves are the eikonal and dynamic results, respectively. All distributions have been normalized to one.

state angular momenta l_f, but not so well at the larger l_f. The sum over l_f is the diffraction dissociation probability, which is rather insensitive to l_{max}.

The differences between the dynamic calculations and the eikonal approximation are most dramatic at 10 MeV/nucleon. The dynamic calculation has a local minimum near $l_f \approx 5$. The position of this minimum increases to larger l_f if we increase the impact parameter b or the velocity v, roughly according to the classical formula $l_{class}=mvb$. The local minimum may reflect the absorption of the valence neutron when it hits the target. We believe that the shoulder beyond the minimum represents neutrons at very low energy in the target frame. We discuss below the linear momentum distributions in order to get more physical insight into this phenomenon.

C. Momentum distributions

The angle-integrated momentum distribution of the neutron with respect to the projectile frame is shown in Fig. 7(a). It shows a broad peak at about 80 MeV/c with a very narrow peak superimposed. The narrow peak is due to a d-wave resonance of the projectile potential, Eq. (1). In actuality there is no such resonance in the ^{11}Be spectrum. This simply shows the limitation of the simple potential model we have used to describe ^{11}Be. It may be seen in comparing the eikonal to the dynamic calculation that the eikonal is remarkably accurate in describing the angle-integrated momentum distribution. It should be noted that models that neglect the final state core-particle interaction will miss resonance peaks such as those found here. The broad peak is rather insensitive to beam energy and the details of the target interaction.

The longitudinal momentum distribution is of considerable interest for several reasons. Of all the momentum distributions, it is least sensitive to the details of the neutron-target interaction. In fact, to some approximation it just reflects the longitudinal momentum content of the initial bound state. However, one feature of the longitudinal momentum distribution, its asymmetry in the projectile frame, is due to the finite duration of the collision and is completely

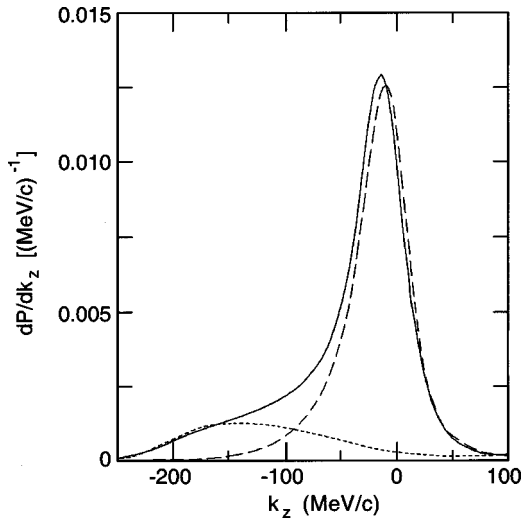

FIG. 8. Longitudinal momentum distribution of neutrons in the rest frame of ^{11}Be produced in diffraction dissociation on a ^{12}C target at 10 MeV/nucleon and an impact parameter $b=8$ fm. The distribution has been separated into two contributions, namely, from low-angular momenta $l_f \leqslant 5$ (long-dashed curve) and high-angular momenta $l_f > 5$ (short-dashed curve). The total distribution (solid curve) includes the interference between the two components.

beyond the scope of the eikonal approximation. This is illustrated in Fig. 7(b) for the diffractive breakup of ^{11}Be on a ^{12}C target at 20 MeV/nucleon and $b=8$ fm. The true distribution is 10% broader than the eikonal, and it has a pronounced tail going to lower momenta with respect to the target.

We saw in Fig. 6 that the angular momentum distribution at 10 MeV/nucleon has a pronounced shoulder for $l_f > 5$. This may be related to a phenomenon seen in the time-dependent Schrödinger dynamics reported in Ref. [22]. The authors found that the neutron can be transferred to a continuum state moving with a velocity close to the target's, calling this the ''towing mode.'' We can examine this in more detail by dividing the neutron wave function into low- and high-angular momentum parts, calculating the longitudinal momentum distribution of each part. The result is shown in Fig. 8. We see that the low-l part is rather symmetric in the projectile frame, but the high-l part has a shifted distribution centered at about -140 MeV/c. This corresponds well to the momentum of neutrons that move slowly with respect to the target nucleus. Thus, we confirm with our model and methods the existence of the towing mode found in Ref. [22].

V. CONCLUSION

Comparing the eikonal to exact dynamics in a model of heavy-ion projectile fragmentation reactions, we find that the eikonal is quite a robust approximation for halo breakup at beam energies as low as 20 MeV/nucleon. Spectroscopy studies using removal cross sections can use the eikonal with a reliability of a few percent for relative cross sections and a few tens of percent for absolute cross sections.

Other reaction phenomena, such as the towing mode that puts the neutron into low energies states with respect to the target, arise in the time development of the reaction and are not accessible in the eikonal. The time-dependent Schrödinger equation seems to offer a good way to calculate such phenomena.

ACKNOWLEDGMENTS

G.B. acknowledges helpful conversations with A. Bonaccorso, D. Brink, P. G. Hansen, W. G. Lynch, and J. A. Tostevin at the ECT* workshop, ''Reaction Mechanisms with Exotic Nuclei.'' This work was supported by the U. S. Department of Energy, Nuclear Physics Division, under Contract Nos. W-31-109-ENG-38 and E-FG-06-90ER-41132.

[1] G. Bertsch, H. Esbensen, and A. Sustich, Phys. Rev. C **42**, 758 (1990).
[2] Y. Ogawa, K. Yabana, and Y. Suzuki, Nucl. Phys. **A543**, 722 (1992).
[3] J.S. Al-Khalili, J.A. Tostevin, and I.J. Thompson, Phys. Rev. C **54**, 1843 (1996).
[4] K. Hencken, G.F. Bertsch, and H. Esbensen, Phys. Rev. C **54**, 3043 (1996).
[5] J.A. Tostevin, J. Phys. G **25**, 735 (1999).
[6] T. Aumann *et al.*, Phys. Rev. Lett. **84**, 35 (2000).
[7] Yu.L. Parfenova, M.V. Zhukov, and J.S. Vaagen, Phys. Rev. C **62**, 044602 (2000).
[8] I. Licot *et al.*, Phys. Rev. C **56**, 250 (1997).
[9] E. Sauvan *et al.*, Phys. Lett. B **491**, 1 (2000).
[10] A. Korsheninnikov *et al.*, Phys. Rev. C **53**, R537 (1996).
[11] C.A. Bertulani and G.F. Bertsch, Phys. Rev. C **49**, 2839 (1994).
[12] H. Esbensen, G.F. Bertsch, and C.A. Bertulani, Nucl. Phys. **A581**, 107 (1995).
[13] H. Esbensen and G.F. Bertsch, Nucl. Phys. **A600**, 37 (1996).
[14] T. Kido, K. Yabana, and Y. Suzuki, Phys. Rev. C **53**, 2296 (1996).
[15] V.S. Melezhik and D. Baye, Phys. Rev. C **59**, 3232 (1999).
[16] M. Fallot, J.A. Scarpaci, D. Lacroix, Ph. Chomaz, and J. Margueron, nucl-th/0101011.
[17] A. Bonaccorso and D.M. Brink, Phys. Rev. C **58**, 2864 (1998).
[18] Y. Sakuragi, M. Yahiro, and M. Kamimura, Prog. Theor. Phys. Suppl. **89**, 136 (1986); Y. Hirabayashi and Y. Sukaragi, Phys. Rev. Lett. **69**, 1892 (1992).
[19] C.A. Bertulani and L.F. Canto, Nucl. Phys. **A539**, 309c (1992).
[20] F.M. Nunes and I.J. Thompson, Phys. Rev. C **59**, 2652 (1999).
[21] H. Esbensen and G.F. Bertsch, Phys. Rev. C **59**, 3240 (1999).
[22] R.L. Varner, W.J. Thompson, T.L. McAbee, E.J. Ludwig, and T.B. Clegg, Phys. Rep. **201**, 57 (1991).
[23] D. Lacroix, J. Scarpaci, and Ph. Chomaz, Nucl. Phys. **A658**, 273 (1999).